

Phenomenological study of the angle between jet axes in heavy-ion collisions

Jin-Wen Kang,¹ Sa Wang,^{2,3} Lei Wang,⁴ and Ben-Wei Zhang^{1,*}

¹Key Laboratory of Quark & Lepton Physics (MOE) and Institute of Particle Physics,
Central China Normal University, Wuhan 430079, China

²College of Science, China Three Gorges University, Yichang 443002, China

³Center for Astronomy & Space Sciences and Institute of Modern Physics,
China Three Gorges University, Yichang 443002, China

⁴School of Applied Physics and Materials, Wuyi University, Jiangmen 529020, China

(Dated: April 17, 2025)

This paper presents a phenomenological study on the angle between the Standard and Winner-Take-All (WTA) jet axes ($\Delta R_{\text{axis}}^{\text{WTA-Std}}$) in high-energy nuclear collisions. The $p+p$ baseline is provided by the PYTHIA8 event generator. The in-medium jet propagation is simulated by the linear Boltzmann transport (LBT) model, which considers both the elastic and inelastic jet-medium interactions. Our theoretical results calculated by the LBT model show that the $\Delta R_{\text{axis}}^{\text{WTA-Std}}$ distribution in Pb+Pb at $\sqrt{s} = 5.02$ TeV is narrower than that in $p+p$, which agrees well with the recent ALICE measurements. The narrowing of $\Delta R_{\text{axis}}^{\text{WTA-Std}}$, which seems to violate the nature of intra-jet broadening due to jet quenching, may be attributed to the influence of “selection bias”. However, the physical details still need to be fully understood. Utilizing a matching-jet method to track the jet evolution in the QGP to remove the selection bias in the Monte Carlo simulations, we observe that the $\Delta R_{\text{axis}}^{\text{WTA-Std}}$ distribution becomes broader due to the jet-medium interactions. At the same time, by rescaling the quark/gluon-jet fractions in Pb+Pb collisions to be the same as that in $p+p$, we find that the fraction change may not significantly influence the modification pattern of jet $\Delta R_{\text{axis}}^{\text{WTA-Std}}$. On the other hand, the selected jet sample in A+A collisions has a significantly narrower initial $\Delta R_{\text{axis}}^{\text{WTA-Std}}$ distribution than the $p+p$ baseline, and such a biased comparison between $p+p$ and A+A conceals the actual intra-jet broadening effect in the experimental measurements. The investigations presented in this paper will deepen our understanding of the relationship between the actual intra-jet modifications in the QGP and the experimental observations.

I. INTRODUCTION

Exploring the properties of the quark-gluon plasma (QGP), a new state of nuclear matter formed at extremely hot and dense conditions, is one of the most important motivations of the heavy-ion collision program at the RHIC and the LHC [1–8]. The high p_T parton or jets generated at a very early stage of the collisions will strongly interact with the medium and dissipate energy when traversing through the QGP, called the “jet quenching” phenomenon. Therefore, jets are widely regarded to be an excellent probe for unveiling the mystery of such deconfined quark soup [9–25]. A series of recently developed jet substructure observables have been used to perform the investigations for further understanding the QGP medium and nucleon structure, including the scaled groomed jet radius θ_g , the groomed jet momentum splitting fraction z_g [26–32], the number of “Soft Drop” branches n_{SD} [27], the radial profile [33–36], the generalised angularities λ_β^k [37], the jet charge Q^k [38, 39], the groomed jet mass [40], the splitting parameter $\sqrt{d_{12}}$, the angular separation ΔR_{12} [41], the N -subjettiness, and the sub-jet fragmentation [42], etc.

Besides the observables mentioned above, there is a fascinating observable—the angle between differently

defined jet axes, ΔR_{axis} , which probes a vast phase space of the jet formation and evolution [43]. The concept of the angle between jet axes ΔR_{axis} was firstly proposed in Ref. [44], in which ΔR_{axis} was calculated at next-to-leading logarithmic accuracy and consistent with the simulations of the Monte Carlo event generators. Subsequently, the ALICE collaboration reported experiment measurements of the angle between jet axes in $p+p$ and Pb+Pb collisions at $\sqrt{s} = 5.02$ TeV [19, 43].

The existing studies show that the physical meanings of the ΔR_{axis} observables are clear and straightforward. ΔR_{axis} measures the geometric distance of two different axes determined by two different algorithms for the same reconstructed jet in the (η, ϕ) plane. Various algorithms determine different jet axes, each with varying degrees of sensitivity to the soft radiation. More specifically, the “Soft Drop” grooming algorithm removes the soft wide-angle radiation in the jets, and the degree of this grooming can be adjusted by parameters [45]. The WTA axis is obtained by reclustering using the “Winner-Take-All” recombination scheme, which tracks the energetic collinear radiation. The WTA axis is typically aligned with the most energetic components of the jet, and the effect of soft radiation is power suppressed in the WTA axis [43, 44]. Systematic discussions of ΔR_{axis} in $p+p$ collisions are performed in Ref. [44].

In nucleus-nucleus collisions, due to the different sensitivity to the soft radiation for different definitions of

* bwzhang@mail.ccnu.edu.cn

the jet axis, the ΔR_{axis} provides a unique opportunity to gain insight into the energy loss mechanisms of jet-medium interactions. Recently the ALICE collaboration has reported the first measurement on the ΔR_{axis} distributions of charged-particle jets in Pb+Pb collisions at $\sqrt{s_{NN}} = 5.02$ TeV [19]. It is found that ΔR_{axis} has narrower distributions in Pb+Pb collisions than in $p+p$. The experimental results show different modification patterns compared to the theoretical calculations with an intra-jet broadening [26]. In Ref. [19], it is implied that the “selection bias” may play an essential role during the jet finding in A+A collisions. In other words, the minimum p_T^{jet} threshold biases the jet selection to favor the candidates with less energy loss [6, 46], but the details in physics are unclear. Moreover, due to the different Casimir color factors ($C_F = 4/3$ for quark and $C_A = 3$ for gluon), the gluon-initiated jets will lose more energy than quark-initiated jets during medium-induced interactions, which leads to a reduced gluon-jet fraction of jet sample in A+A collisions [38, 39, 47]. Since the gluon-jet is expected to interact more with the QGP medium, Ref. [19] suggests that the reduced gluon-jet fraction (from an alternative perspective, a relatively enhanced quark-jet fraction) is believed to be the main reason for the narrower ΔR_{axis} distribution in Pb+Pb collisions compared to the vacuum case. Further detailed theoretical explorations are necessary to disentangle the influences of the selection bias and the quark/gluon-jet fraction changes to the observation in the experiment, which is essential to understand the relationship between the actual intra-jet modifications in the QGP and the experimental observations.

This paper presents a theoretical study on the angle between the Standard and WTA jet axes ($\Delta R_{\text{axis}}^{\text{WTA-Std}}$) in high-energy nuclear collisions. The $p+p$ baseline is provided by the PYTHIA8 event generator, and the in-medium jet propagation is simulated by the linear Boltzmann transport (LBT) model. We will perform the calculations of the $\Delta R_{\text{axis}}^{\text{WTA-Std}}$ distribution in Pb+Pb at $\sqrt{s} = 5.02$ TeV compared to the recently reported ALICE measurements. Furthermore, we will investigate the influences of the event “selection bias” and the quark/gluon-jet fraction changes to the modification patterns of $\Delta R_{\text{axis}}^{\text{WTA-Std}}$ distribution in nucleus-nucleus collisions. We will use the “matching-jet” method to track the jet evolution in the QGP, in which the realistic jet modification can be unveiled. In addition, we will perform a detailed analysis to demonstrate that the critical factor concealing such intra-jet broadening effects in experimental measurement is the biased comparison between two jet samples in $p+p$ and Pb+Pb collisions. At the same time, the influence of the quark/gluon-jet fraction changes is limited.

The rest of this article is structured as follows. In Sec. II, we introduce the theoretical framework utilized to study the medium modification of $\Delta R_{\text{axis}}^{\text{WTA-Std}}$ in high-energy nuclear collisions. We show our calculated re-

sults and discussions in Sec. III. At last, we summarize this work in Sec. IV.

II. FRAMEWORK

When employing different reclustering/grooming algorithms to process a given jet, we will get some new jets slightly different from the original one. The ΔR_{axis} is a novel infrared and collinear (IRC) safe jet-substructure observable proposed in Ref. [44] to study the angular distance between the two jet axes defined with different jet algorithms:

$$\Delta R_{\text{axis}}^{a-b} = \sqrt{(y_{\text{axis}}^a - y_{\text{axis}}^b)^2 + (\phi_{\text{axis}}^a - \phi_{\text{axis}}^b)^2}, \quad (1)$$

where a and b denote any two different axis algorithms, y and ϕ are the rapidity and the azimuthal angle. According to different reclustering/grooming algorithms, three types of ΔR_{axis} combination are extensively investigated in jet physics at the LHC [19, 37, 43, 44]: WTA–Standard, WTA–SoftDrop and Standard–SoftDrop. This work will focus on the angle between the Standard and WTA axes.

At the LHC, almost universally employed the anti- k_t algorithm [48] to reconstruct jets [49], so we call the jet axis obtained using the anti- k_t algorithm (with default E recombination scheme) clustering as the “Standard” axis. The WTA is a recombination scheme that specifies how to combine the momenta when merging two subbranches during the clustering procedure. Specifically, we directly assign the transverse momentum sum of the two subbranches as the transverse momentum of the merged branch and designate the direction of the harder of two subbranches as the direction of the merged branch [43, 50],

$$\begin{aligned} p_{T,r} &= p_{T,i} + p_{T,j}, \\ \phi_r &= \phi_k, \\ y_r &= y_k, \\ k &= \begin{cases} i & p_{T,i} > p_{T,j} \\ j & p_{T,i} < p_{T,j} \end{cases}, \end{aligned}$$

where the subscript r denotes the merged branch; i and j denote the two prongs, respectively. The WTA scheme is infrared/collinear safe and can powerfully suppress the effect of soft radiation [43, 44]. Because of these features, the WTA scheme has been used to study jet-like event shapes [50], recoil-free observables [51, 52], flavor identification of jets [53], etc. Back to our work, we recluster the constituents of the “Standard” jet using the C/A algorithm [54, 55] with the WTA p_T recombination scheme, and then we can get the WTA axis.

A Monte Carlo event generator PYTHIA v8.309 [56] with Monash 2013 [57] tune is used to simulate jet productions in $p+p$ collisions as the baseline. We use

charged-particles with $p_T > 0.15$ GeV/c and pseudo-rapidity range $|\eta| < 0.9$ to reconstruct jets. All jets are reconstructed by the anti- k_t algorithm with the E recombination scheme and the distance parameter $R = 0.2$ using FASTJET v3.4.0 package [58, 59].

We employ the linear Boltzmann transport (LBT) model [60–63] to simulate both elastic and inelastic scattering processes of the jet shower partons and the thermal recoil partons in the QGP medium. The LBT model performed well in a series of jet quenching measurements, which was highly consistent with the experimental results [60, 62–65]. In the LBT model, the linear Boltzmann transport equation is used to describe the elastic scattering process,

$$p_1 \cdot \partial f_1(p_1) = - \int \frac{d^3 p_2}{(2\pi)^3 2E_2} \int \frac{d^3 p_3}{(2\pi)^3 2E_3} \int \frac{d^3 p_4}{(2\pi)^3 2E_4} \times \frac{1}{2} \sum_{2(3,4)} (f_1 f_2 - f_3 f_4) |\mathcal{M}_{12 \rightarrow 34}|^2 (2\pi)^4 \times S_2(\hat{s}, \hat{t}, \hat{u}) \delta^{(4)}(p_1 + p_2 - p_3 - p_4), \quad (2)$$

where $f_i(p_i)$ ($i = 1, 2, 3, 4$) are the phase-space distribution of partons that participate in the reaction; $|\mathcal{M}_{12 \rightarrow 34}|^2$ is the leading-order (LO) elastic scattering matrix elements [66, 67]; in order to avoid possible collinear divergence of $|\mathcal{M}_{12 \rightarrow 34}|^2$ for massless partons, here, a Lorentz-invariant regularization condition $S_2(\hat{s}, \hat{t}, \hat{u}) \equiv \theta(\hat{s} \geq 2\mu_D^2) \theta(-\hat{s} + \mu_D^2 \leq \hat{t} \leq -\mu_D^2)$ is introduced [68]; μ_D^2 is the Debye screening mass. It should be noted that the medium response effect is included in the LBT model during our simulations. The higher-twist approach [69–73] describes the inelastic scattering of medium-induced gluon radiation,

$$\frac{dN_g}{dx dk_\perp^2 dt} = \frac{2\alpha_s C_A P(x) \hat{q}}{\pi k_\perp^4} \left(\frac{k_\perp^2}{k_\perp^2 + x^2 m^2} \right)^4 \sin^2 \left(\frac{t - t_i}{2\tau_f} \right), \quad (3)$$

where x is the energy fraction of the emitted gluon taken from its parent parton with mass m , k_\perp is the transverse momentum of the radiated gluon, $P(x)$ is the splitting function, \hat{q} is the jet transport coefficient (specific details can be found in Ref [61]), and τ_f is the formation time of the radiated gluons in the QGP medium. The background hydrodynamic profile for the bulk QGP medium is provided by simulations from the 3+1D MUSIC relativistic second-order viscous hydro model [74–76] with the averaged initial condition from the 3D TRENTO model [77, 78]. The evolution of the background medium was carried out in a few key steps. First, we employed the 3D TRENTO model to generate about 2000 event-by-event initial conditions for the most central 0-10% of Pb+Pb collisions at $\sqrt{s_{NN}} = 5.02$ TeV. Next, we averaged these initial conditions to obtain the average initial state profile. Ignoring the evolution of the pre-equilibrium stage, we directly used the averaged initial-state condition as the input for the 3+1D MUSIC

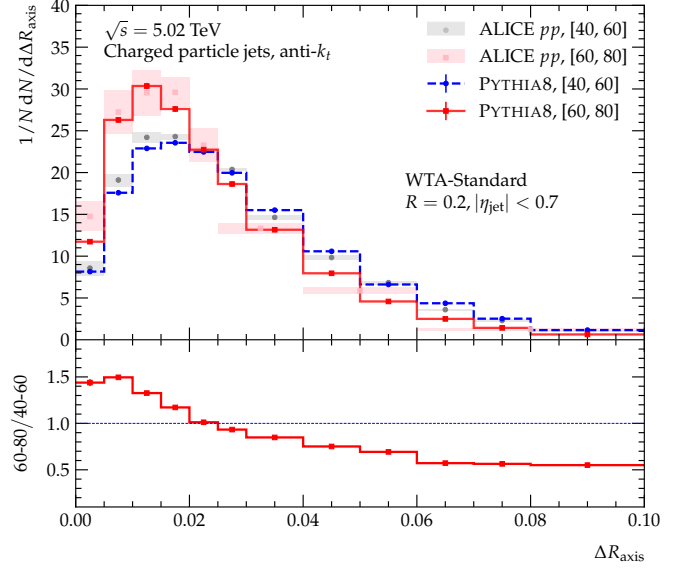


FIG. 1. Normalized distributions of the angle between the Standard and WTA axes $\Delta R_{\text{axis}}^{\text{WTA-Std}}$ of inclusive jets calculated by the PYTHIA in $p+p$ collisions at $\sqrt{s_{NN}} = 5.02$ TeV within two p_T ranges: $40 < p_T < 60$ GeV/c and $60 < p_T < 80$ GeV/c, are compared to the ALICE data [19]. The ratio of these two p_T ranges is also plotted in the lower panel.

model to simulate the evolution of the QGP medium. Consequently, our current framework does not include event-by-event fluctuations [79] or pre-equilibrium effects.

After the evolutions of the parton shower in the medium are completed, we need to perform hadronization to obtain the hadron-level events that can be observed in the experiment. In this work, we first construct strings using the colorless method from the JETSCAPE framework based on minimization criteria [80] and then perform hadronization and hadron decays using the Lund string model [56, 81, 82] provided by PYTHIA. The JETSCAPE collaboration has already demonstrated in works [32, 83] that this model is reliable.

III. RESULTS AND DISCUSSIONS

To calibrate the $p+p$ baseline of our study, in Figure 1, we firstly show the normalized distributions of the angle between the Standard and WTA axes $\Delta R_{\text{axis}}^{\text{WTA-Std}}$ of inclusive jets calculated by the PYTHIA in $p+p$ collisions at $\sqrt{s} = 5.02$ TeV within two p_T ranges $40 < p_T < 60$ GeV/c and $60 < p_T < 80$ GeV/c compared to the ALICE data. It is found that the calculations of PYTHIA can describe the ALICE data for these two p_T ranges. By taking the ratio of these two p_T ranges in the lower panel, we find that jets with $60 < p_T < 80$ GeV/c have a narrower $\Delta R_{\text{axis}}^{\text{WTA-Std}}$ distribution than those with $40 < p_T < 60$ GeV/c, which indicates that higher- p_T jets

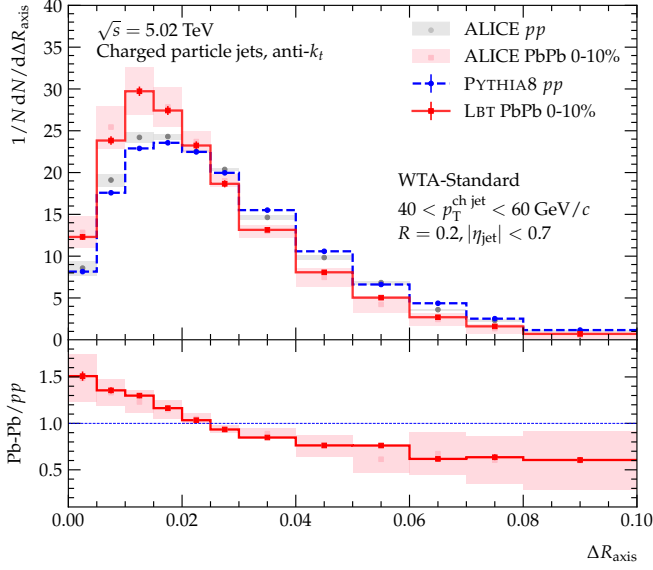


FIG. 2. Normalized $\Delta R_{\text{axis}}^{\text{WTA-Std}}$ distributions for inclusive jets in $p+p$ and Pb+Pb collisions at $\sqrt{s_{NN}} = 5.02$ TeV, including the results of theoretical calculation and ALICE experimental data [19]. The ratios are also plotted in the lower panel.

usually have a narrower $\Delta R_{\text{axis}}^{\text{WTA-Std}}$ than the lower- p_T ones.

Now we proceed to the calculations of $\Delta R_{\text{axis}}^{\text{WTA-Std}}$ distribution in nucleus-nucleus collisions. In Figure 2, we show the normalized $\Delta R_{\text{axis}}^{\text{WTA-Std}}$ distribution in $p+p$ and 0-10% Pb+Pb collisions at $\sqrt{s_{NN}} = 5.02$ TeV compared to the recent reported ALICE data [19]. At the same time, the ratios of PbPb/ pp are also shown in the lower panel. Our theoretical results can reasonably describe the experimental data in both $p+p$ and Pb+Pb collisions and the PbPb/ pp ratio. We observe that the $\Delta R_{\text{axis}}^{\text{WTA-Std}}$ distribution in Pb+Pb collisions is narrower than that in $p+p$ which indicates the two jet axes are closer for the jet sample in Pb+Pb compared to that in $p+p$.

Generally, the same minimum and maximum p_T thresholds (e.g. $40 < p_T^{\text{jet}} < 60$ GeV/ c) are imposed to select the jet samples both in $p+p$ and A+A collisions. The comparison of these two jet samples provides valuable information about the in-medium jet modification relative to the vacuum case. However, if only considering the jet-medium interaction but not the “selection biases” in the theoretical calculations and experimental measurements, we cannot fully understand the relationship between the energy loss mechanisms and the observables [46]. Consider a jet (unquenched jet) generated in the initial hard scattering, passing through the QGP medium and losing energy due to interaction with the medium, becoming a medium-modified jet (quenched jet). According to the transverse momentum values before and after the energy loss of this jet, we can place this jet in the lower triangle shadow area in Figure 3. In usual experimental and phenomenological

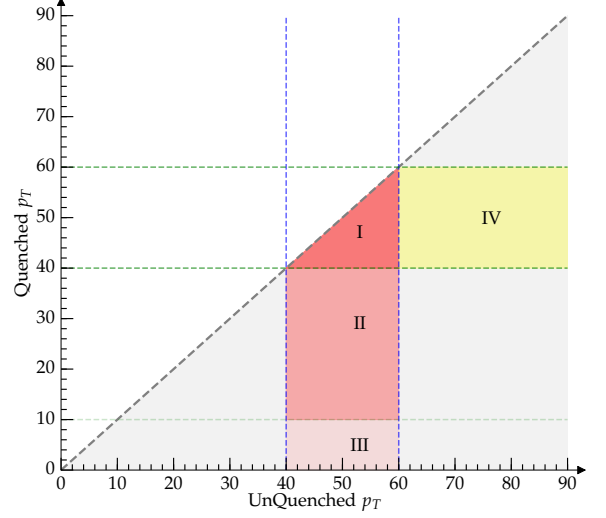


FIG. 3. Schematic of the selection bias. The horizontal axis corresponds to the transverse momentum of the unquenched jets, and the vertical axis corresponds to the quenched jets’ transverse momentum. Effective jets exist only in the shaded area of the lower triangle.

studies of the current, the selected sample of $p+p$ events, which is the unquenched jets sample, is located in the I+II+III region in Figure 3. The selected jet sample in heavy-ion collisions, the quenched jets, is in the I+IV region in Figure 3. This means the traditional selection method of unquenched and quenched jet samples is significantly biased. We note that the area I corresponds to the jets survived in the selection window (40–60 GeV/ c) after in-medium energy loss. Moreover, area IV corresponds to jets with higher p_T (> 60 GeV/ c) but finally falls in the selection window due to the evident energy loss.

The selection bias effect often plays an important role in the studies of nuclear modification in heavy-ion collisions. One can find the related investigations in Refs. [6, 34, 46, 84–90]. We have noticed that there have been a lot of research (e.g. [88–97]) attempts to eliminate or reduce the impact of selection bias on the studies of nuclear modifications. Some experimentalists have suggested that the issue of selection bias could be resolved by canceling the transverse momentum cut on the jet spectrum [94–97]. In addition, one can efficiently track the jet evolution in the Monte Carlo simulations for the theoretical models. In this work, we study the influence of selection bias on our concerned observable from the effect of jet modification using a “matching-jet” method, first proposed in Refs. [88, 90]. Specifically, in the two hadron-level inclusive jet samples, quenched and unquenched, we pair two jets whose distance in the (η, ϕ) plane is less than the jet radius R before and after quenching, considering them as the unquenched

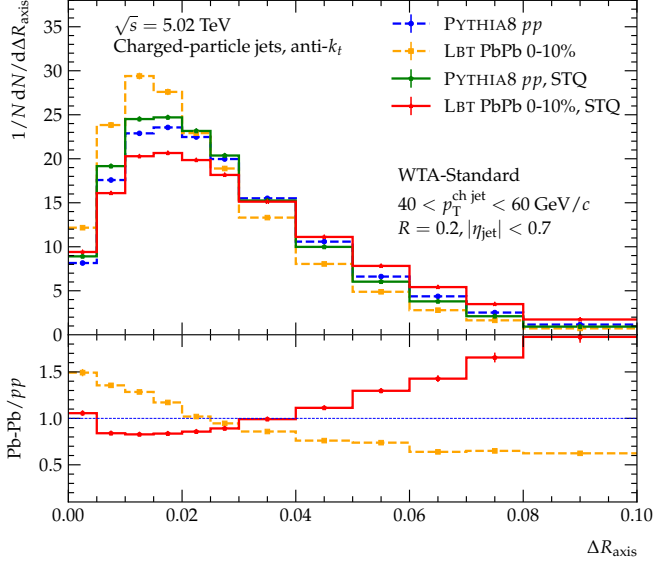


FIG. 4. Normalized $\Delta R_{\text{axis}}^{\text{WTA-Std}}$ distributions of the selected jet samples in $p+p$ and 0-10% Pb+Pb collisions at $\sqrt{s_{NN}} = 5.02$ TeV. STQ represents the calculations with matching-jet method. The ratios are also plotted in the lower panel.

and quenched versions of the same jet. To minimize the omission of jets that have experienced sizeable energy loss, we have appropriately reduced the transverse momentum threshold in the reconstruction of quenched jets ($p_T > 10$ GeV) to take into account the region of I and II in Figure 3. Since the contribution of region III is small, and the matching efficiency in this region is poor, we neglect this region in the matching procedure. The matching procedure lets us focus on the jet-by-jet comparison before and after the in-medium evolution. Although this method makes it difficult to consider the effects of the nuclear parton distribution function and could not be applied to experimental measurements, it gives us a new perspective to study the medium modification of the angle between the Standard and WTA jet axes.

In Figure 4, we show the distributions of $\Delta R_{\text{axis}}^{\text{WTA-Std}}$ for samples of matched jets in the region I+II. For comparison, the Monte Carlo simulation results shown in Figure 2 have also been added to this figure. For the convenience of the following discussion, we labeled these matched jets by Select-Then-Quench (STQ), a matching-jet method first introduced in Ref. [88]. Since the jets are well-tracked in the matching procedure, comparing the STQ (pp) and STQ (PbPb) cases reveals the actual jet modification in the QGP, in which the influences of selection bias are almost removed. We observe that the $\Delta R_{\text{axis}}^{\text{WTA-Std}}$ distribution of STQ (PbPb) shows evident broadening compared to that of STQ (pp), and the PbPb/ pp ratio of STQ is enhanced at $\Delta R_{\text{axis}} > 0.04$. It means the jets get broader by the interactions with the QGP medium compared to their initial structures.

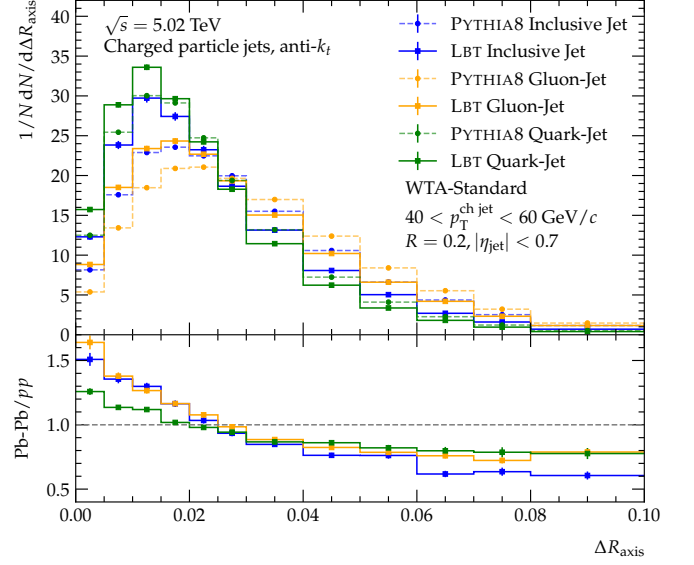


FIG. 5. Normalized $\Delta R_{\text{axis}}^{\text{WTA-Std}}$ distributions of the quark-jets, gluon-jets and inclusive jets in $p+p$ and 0-10% Pb+Pb collisions at $\sqrt{s_{NN}} = 5.02$ TeV. The ratios are also plotted in the lower panel.

However, the modification patterns of STQ results are inverse to the normal theoretical calculation, while the latter contains the effect of selection bias. Now, we can conclude that the selection bias obscures the real nature of intra-jet broadening and leads to a narrowed modification of the $\Delta R_{\text{axis}}^{\text{WTA-Std}}$ distribution. Many researchers have been focused on searching for medium-induced intra-jet broadening [26, 60], and recent experimentalists have also reported some positive signals [95–97].

This simple test above demonstrates the importance of selection bias in studying the nuclear modification of the ΔR_{axis} distribution. However, please note that although we have excluded selection bias using the STQ method, this also obscures the quark-initiated jets' fraction increase effect that existed in experiments or conventional Monte Carlo studies, where the proportion of quark-initiated jets tends to increase because gluons usually lose more energy [98–100]. In Monte Carlo studies, we can distinguish whether the jet is a quark- or gluon-jet by comparing the distance between the jet and the initial outgoing hard partons in the (η, ϕ) plane. Utilizing this method, we have employed the PYTHIA8 event generator to ascertain that the quark- and gluon-jet fractions of inclusive jets in $p+p$ collisions at $\sqrt{s} = 5.02$ TeV at leading-order (LO) accuracy are about 36.7% and 63.3% with jet radius $R = 0.2$, $|\eta_{\text{jet}}| < 0.7$ and $40 < p_T^{\text{ch jet}} < 60$ GeV/c. To test the flavor dependence of jet ΔR_{axis} and its medium modification, as shown in Figure 5, we estimate the ΔR_{axis} distributions of quark-jets, gluon-jets and inclusive jets in $p+p$ and 0-10% Pb+Pb collisions at $\sqrt{s_{NN}} = 5.02$ TeV. The quark-jets exhibit a narrower initial ΔR_{axis} distribu-

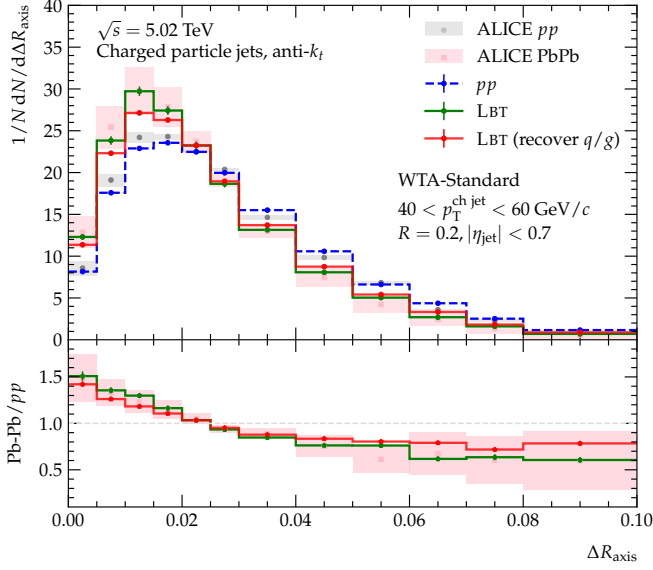


FIG. 6. The LBT calculations of $\Delta R_{\text{axis}}^{\text{WTA-Std}}$ distributions in Pb+Pb collisions with recovered quark/gluon-jet fractions are compared with the normal LBT calculations and the ALICE data. The ratios are also plotted in the lower panel.

tion than the gluon-jets. In Pb+Pb collisions, we find that both the quark- and gluon-jets become narrower than in $p+p$, and the narrowing of the latter is more substantial. Moreover, the ΔR_{axis} modification of inclusive jets seems closer to that of the gluon-jets sample.

To test the influence of the quark/gluon-jet fraction change on the $\Delta R_{\text{axis}}^{\text{WTA-Std}}$ modification, we rescale their fractions in Pb+Pb collisions to be consistent with their initial fraction (36.7% and 63.3%). The calculations with rescaled quark/gluon-jet fractions, denoted as LBT (recover q/g), are shown in Figure 6 and compared to the normal LBT calculations as well as the ALICE data. We find that the calculations with rescaled fractions do not significantly differ from the normal LBT calculations. Since the rescaled calculations exclude the influence of the fraction changes, it hints that the decreased gluon-jet fraction is not the main reason that leads to a narrowing ΔR_{axis} distribution of inclusive jet in Pb+Pb collisions.

To find out the actual jet modification, in Figure 4, we have compared the selected jet sample with $40 < p_T < 60$ GeV in $p+p$ collisions with its quenched counterpart in Pb+Pb collisions using the matching-jet method. Similarly, we can also trace the initial counterpart of the jet sample with $40 < p_T < 60$ GeV selected in Pb+Pb collisions. We denote such matched initial counterpart as $pp(\text{matched})$ for simplicity. In Figure 7, the $\Delta R_{\text{axis}}^{\text{WTA-Std}}$ distribution of the selected jet sample with $40 < p_T < 60$ GeV in Pb+Pb is compared to its initial counterpart, the $pp(\text{matched})$, and the one with $40 < p_T < 60$ GeV selected in $p+p$ collisions; the ratios of PbPb/pp and $\text{PbPb}/pp(\text{matched})$ are also plotted in the lower panel. We find that $pp(\text{matched})$ has a significantly narrower

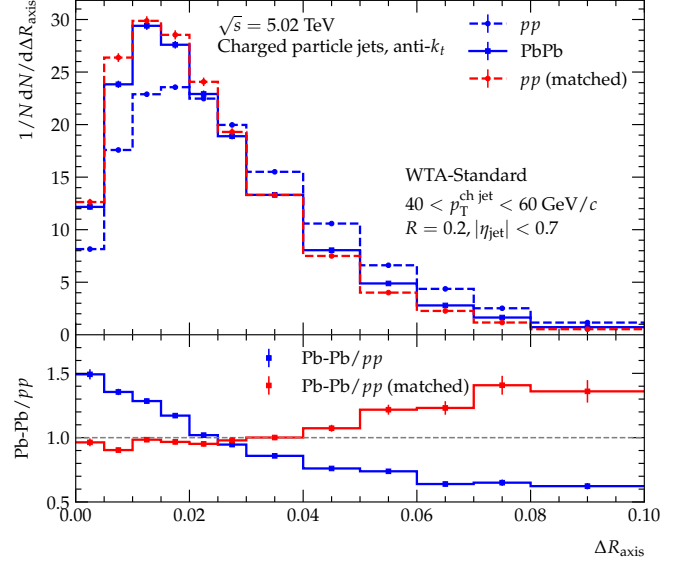


FIG. 7. The $\Delta R_{\text{axis}}^{\text{WTA-Std}}$ distribution of the selected jet sample with $40 < p_T < 60$ GeV in Pb+Pb is compared to its initial counterpart, denoted as $pp(\text{matched})$, and that selected in $p+p$ collisions, the ratios of PbPb/pp and $\text{PbPb}/pp(\text{matched})$ are also plotted in the lower panel.

distribution than the $p+p$. The jet sample selected in A+A collisions after jet quenching usually has higher initial p_T , while the one with higher p_T usually has narrower $\Delta R_{\text{axis}}^{\text{WTA-Std}}$ as shown in Figure 1. When taking the ratio of Pb+Pb to their initial counterpart, we can observe a broadening in $\Delta R_{\text{axis}}^{\text{WTA-Std}}$ as shown in the lower panel of Figure 7. However, if we only compare the jet samples with $40 < p_T < 60$ GeV selected independently in $p+p$ and Pb+Pb collisions, the broadening turns into narrowing. In other words, when taking the ratio of PbPb/pp in the ALICE measurements, the selected jet sample in A+A collisions has a significantly narrower initial $\Delta R_{\text{axis}}^{\text{WTA-Std}}$ distribution than the $p+p$ baseline. Such a biased comparison between $p+p$ and A+A might conceal the real intra-jet broadening behavior during the jet quenching.

Finally, another point to note is that our work has not considered nPDFs effects in the Pb+Pb collision simulations. Our study investigated how cold nuclear effects affect $\Delta R_{\text{axis}}^{\text{WTA-Std}}$ distributions in Pb+Pb collisions. The overall trend of nuclear modification showed no significant difference whether we included these cold nuclear effects in the model or not. To facilitate the application of the “matching-jet” method for matching Pb+Pb events with $p+p$ references, we deliberately omitted nPDF effects in this work.

IV. SUMMARY

In this work, we study the angle between the Standard and Winner-Take-All jet axes $\Delta R_{\text{axis}}^{\text{WTA-Std}}$ in $p+p$ and 0-10% Pb+Pb collisions at $\sqrt{s_{NN}} = 5.02$ TeV. We mainly investigate the influences of selection bias and the quark/gluon-jet fraction changes on the modification patterns of the $\Delta R_{\text{axis}}^{\text{WTA-Std}}$ distribution in Pb+Pb collisions. The initial $\Delta R_{\text{axis}}^{\text{WTA-Std}}$ distribution in $p+p$ collisions is calculated by the PYTHIA8 event generator. The in-medium jet propagation in nucleus-nucleus collisions is simulated by the LBT model, which considers both the elastic and inelastic jet-medium interactions.

Firstly, our theoretical results calculated by the LBT model show that the $\Delta R_{\text{axis}}^{\text{WTA-Std}}$ distribution in Pb+Pb at $\sqrt{s} = 5.02$ TeV is narrower than that in $p+p$, which agrees well with the recently reported ALICE measurements. However, the narrowing of $\Delta R_{\text{axis}}^{\text{WTA-Std}}$ seems to violate the nature of intra-jet broadening due to jet quenching. The phenomenon may be attributed to “selection bias”, which skews the jet selection process by preferentially including candidates that exhibit less energy loss in A+A collisions. Utilizing a matching-jet method to track the jet evolution in the QGP to reduce the selection bias in the Monte Carlo simulations, we observe that the $\Delta R_{\text{axis}}^{\text{WTA-Std}}$ distribution becomes broader due to the jet-medium interactions. At the same time, by rescaling the quark/gluon-jet fractions in Pb+Pb collisions to be the same as that in $p+p$, we find that the

fraction change may not significantly influence the modification pattern of jet $\Delta R_{\text{axis}}^{\text{WTA-Std}}$. On the other hand, we find that the selected jet sample in A+A collisions has a significantly narrower initial $\Delta R_{\text{axis}}^{\text{WTA-Std}}$ distribution than the $p+p$ baseline, and such a biased comparison between $p+p$ and A+A might conceal the actual intra-jet broadening effect in the experimental measurements. The investigations presented in this paper will deepen our understanding of the relationship between the actual intra-jet modifications in the QGP and the experimental observations. However, the methodology currently utilized in this study cannot be directly applied to experimental measurements. Recently, we have noticed that Z/γ -tagged jets or high- p_T -hadron-tagged jets can be used to reduce selection bias and can apply to real experimental measurements [95–97, 101, 102]. Specifically, by using tagger particles rather than jets for event selection, the selection bias is only induced by the choice of tagger. Since tagger particles do not interact with the QGP medium, this approach significantly reduces the impact of selection bias on jet quenching studies. Our future research will employ Z/γ -tagged jets to minimize selection bias and explore intra-jet broadening phenomena in heavy-ion collisions.

Acknowledgments: This research is supported by the Guangdong Major Project of Basic and Applied Basic Research No. 2020B0301030008, and the National Natural Science Foundation of China with Project Nos. 11935007, 12035007 and 12247127. S. Wang is supported by China Postdoctoral Science Foundation under project No. 2021M701279.

-
- [1] B. A. Freedman and L. D. McLerran, *Phys. Rev. D* **16**, 1169 (1977).
 - [2] E. V. Shuryak, *Sov. Phys. JETP* **47**, 212 (1978).
 - [3] M. Connors, C. Nattrass, R. Reed, and S. Salur, *Rev. Mod. Phys.* **90**, 025005 (2018), [arXiv:1705.01974 \[nucl-ex\]](#).
 - [4] J.-P. Blaizot and Y. Mehtar-Tani, *Int. J. Mod. Phys. E* **24**, 1530012 (2015), [arXiv:1503.05958 \[hep-ph\]](#).
 - [5] P. Braun-Munzinger, V. Koch, T. Schäfer, and J. Stachel, *Phys. Rept.* **621**, 76 (2016), [arXiv:1510.00442 \[nucl-th\]](#).
 - [6] L. Cunqueiro and A. M. Sickles, *Prog. Part. Nucl. Phys.* **124**, 103940 (2022), [arXiv:2110.14490 \[nucl-ex\]](#).
 - [7] S. Cao and G.-Y. Qin, *Ann. Rev. Nucl. Part. Sci.* **73**, 205 (2023), [arXiv:2211.16821 \[nucl-th\]](#).
 - [8] L. Apolinário, Y.-J. Lee, and M. Winn, *Prog. Part. Nucl. Phys.* **127**, 103990 (2022), [arXiv:2203.16352 \[hep-ph\]](#).
 - [9] X.-N. Wang and M. Gyulassy, *Phys. Rev. Lett.* **68**, 1480 (1992).
 - [10] M. Gyulassy, I. Vitev, X.-N. Wang, and B.-W. Zhang, “Jet quenching and radiative energy loss in dense nuclear matter,” in *Quark CGluon Plasma 3*, edited by R. C. Hwa and X.-N. Wang (World Scientific, 2004) pp. 123–191, [arXiv:nucl-th/0302077](#).
 - [11] Y. Mehtar-Tani, J. G. Milhano, and K. Tywoniuk, *Int. J. Mod. Phys. A* **28**, 1340013 (2013), [arXiv:1302.2579 \[hep-ph\]](#).
 - [12] G.-Y. Qin and X.-N. Wang, *Int. J. Mod. Phys. E* **24**, 1530014 (2015), [arXiv:1511.00790 \[hep-ph\]](#).
 - [13] X.-N. Wang, *Phys. Rev. C* **58**, 2321 (1998), [arXiv:hep-ph/9804357](#).
 - [14] E. Wang and X.-N. Wang, *Phys. Rev. Lett.* **87**, 142301 (2001), [arXiv:nucl-th/0106043](#).
 - [15] E. Wang and X.-N. Wang, *Phys. Rev. Lett.* **89**, 162301 (2002), [arXiv:hep-ph/0202105](#).
 - [16] I. Vitev and B.-W. Zhang, *Phys. Rev. Lett.* **104**, 132001 (2010), [arXiv:0910.1090 \[hep-ph\]](#).
 - [17] R. B. Neufeld, I. Vitev, and B. W. Zhang, *Phys. Rev. C* **83**, 034902 (2011), [arXiv:1006.2389 \[hep-ph\]](#).
 - [18] Y. He, L.-G. Pang, and X.-N. Wang, *Phys. Rev. Lett.* **125**, 122301 (2020), [arXiv:2001.08273 \[hep-ph\]](#).
 - [19] S. Acharya *et al.* (ALICE), (2023), [arXiv:2303.13347 \[nucl-ex\]](#).
 - [20] J.-W. Kang, L. Wang, W. Dai, S. Wang, and B.-W. Zhang, (2023), [arXiv:2304.04649 \[nucl-th\]](#).
 - [21] W. Dai, I. Vitev, and B.-W. Zhang, *Phys. Rev. Lett.* **110**, 142001 (2013), [arXiv:1207.5177 \[hep-ph\]](#).
 - [22] Z. Yang, Y. He, I. Moulton, and X.-N. Wang, *Phys. Rev. Lett.* **132**, 011901 (2024), [arXiv:2310.01500 \[hep-ph\]](#).
 - [23] S. Wang, W. Dai, E. Wang, X.-N. Wang, and B.-W. Zhang, *Symmetry* **15**, 727 (2023), [arXiv:2303.14660 \[nucl-th\]](#).

- [24] M. Xie, W. Ke, H. Zhang, and X.-N. Wang, *Phys. Rev. C* **108**, L011901 (2023), [arXiv:2206.01340 \[hep-ph\]](#).
- [25] Z. Yang, T. Luo, W. Chen, L.-G. Pang, and X.-N. Wang, *Phys. Rev. Lett.* **130**, 052301 (2023), [arXiv:2203.03683 \[hep-ph\]](#).
- [26] F. Ringer, B.-W. Xiao, and F. Yuan, *Phys. Lett. B* **808**, 135634 (2020), [arXiv:1907.12541 \[hep-ph\]](#).
- [27] S. Acharya *et al.* (ALICE), *Phys. Lett. B* **802**, 135227 (2020), [arXiv:1905.02512 \[nucl-ex\]](#).
- [28] S. Acharya *et al.* (ALICE), *Phys. Rev. Lett.* **128**, 102001 (2022), [arXiv:2107.12984 \[nucl-ex\]](#).
- [29] L. Wang, J.-W. Kang, Q. Zhang, S. Shen, W. Dai, B.-W. Zhang, and E. Wang, *Chin. Phys. Lett.* **40**, 032101 (2023), [arXiv:2211.13674 \[nucl-th\]](#).
- [30] G. Aad *et al.* (ATLAS), *Phys. Rev. C* **107**, 054909 (2023), [arXiv:2211.11470 \[nucl-ex\]](#).
- [31] Q. Zhang, Z.-X. Xu, W. Dai, B.-W. Zhang, and E. Wang, (2023), [arXiv:2303.08620 \[nucl-th\]](#).
- [32] Y. Tachibana *et al.* (JETSCAPE), (2023), [arXiv:2301.02485 \[hep-ph\]](#).
- [33] Y. Li, S. Wang, and B.-W. Zhang, *Phys. Rev. C* **108**, 024905 (2023), [arXiv:2209.00548 \[hep-ph\]](#).
- [34] S. Wang, W. Dai, B.-W. Zhang, and E. Wang, *Chin. Phys. C* **45**, 064105 (2021), [arXiv:2012.13935 \[nucl-th\]](#).
- [35] S. Wang, W. Dai, J. Yan, B.-W. Zhang, and E. Wang, *Nucl. Phys. A* **1005**, 121787 (2021), [arXiv:2001.11660 \[nucl-th\]](#).
- [36] S. Wang, W. Dai, B.-W. Zhang, and E. Wang, *Eur. Phys. J. C* **79**, 789 (2019), [arXiv:1906.01499 \[nucl-th\]](#).
- [37] R. Ehlers (ALICE), *PoS ICHEP2022*, 460 (2022), [arXiv:2211.11800 \[nucl-ex\]](#).
- [38] S.-Y. Chen, B.-W. Zhang, and E.-K. Wang, *Chin. Phys. C* **44**, 024103 (2020), [arXiv:1908.01518 \[nucl-th\]](#).
- [39] A. M. Sirunyan *et al.* (CMS), *JHEP* **07**, 115 (2020), [arXiv:2004.00602 \[hep-ex\]](#).
- [40] A. M. Sirunyan *et al.* (CMS), *JHEP* **10**, 161 (2018), [arXiv:1805.05145 \[hep-ex\]](#).
- [41] G. Aad *et al.* (ATLAS), *Phys. Rev. Lett.* **131**, 172301 (2023), [arXiv:2301.05606 \[nucl-ex\]](#).
- [42] J. Mulligan (ALICE), *PoS EPS-HEP2021*, 298 (2022), [arXiv:2110.05411 \[nucl-ex\]](#).
- [43] S. Acharya *et al.* (ALICE), *JHEP* **07**, 201 (2023), [arXiv:2211.08928 \[nucl-ex\]](#).
- [44] P. Cal, D. Neill, F. Ringer, and W. J. Waalewijn, *JHEP* **04**, 211 (2020), [arXiv:1911.06840 \[hep-ph\]](#).
- [45] A. J. Larkoski, S. Marzani, G. Soyez, and J. Thaler, *JHEP* **05**, 146 (2014), [arXiv:1402.2657 \[hep-ph\]](#).
- [46] T. Renk, *Phys. Rev. C* **88**, 054902 (2013), [arXiv:1212.0646 \[hep-ph\]](#).
- [47] H. T. Li and I. Vitev, *Phys. Rev. D* **101**, 076020 (2020), [arXiv:1908.06979 \[hep-ph\]](#).
- [48] M. Cacciari, G. P. Salam, and G. Soyez, *JHEP* **04**, 063 (2008), [arXiv:0802.1189 \[hep-ph\]](#).
- [49] R. Gauld, A. Huss, and G. Stagnitto, *Phys. Rev. Lett.* **130**, 161901 (2023), [arXiv:2208.11138 \[hep-ph\]](#).
- [50] D. Bertolini, T. Chan, and J. Thaler, *JHEP* **04**, 013 (2014), [arXiv:1310.7584 \[hep-ph\]](#).
- [51] A. J. Larkoski, D. Neill, and J. Thaler, *JHEP* **04**, 017 (2014), [arXiv:1401.2158 \[hep-ph\]](#).
- [52] D. Neill, A. Papaefstathiou, W. J. Waalewijn, and L. Zoppi, *JHEP* **01**, 067 (2019), [arXiv:1810.12915 \[hep-ph\]](#).
- [53] S. Caletti, A. J. Larkoski, S. Marzani, and D. Reichelt, *JHEP* **10**, 158 (2022), [arXiv:2205.01117 \[hep-ph\]](#).
- [54] Y. L. Dokshitzer, G. D. Leder, S. Moretti, and B. R. Webber, *JHEP* **08**, 001 (1997), [arXiv:hep-ph/9707323](#).
- [55] M. Wobisch and T. Wengler, in *Workshop on Monte Carlo Generators for HERA Physics (Plenary Starting Meeting)* (1998) pp. 270–279, [arXiv:hep-ph/9907280](#).
- [56] C. Bierlich *et al.*, *SciPost Phys. Codebases* **8** (2022), 10.21468/SciPostPhysCodeb.8, [arXiv:2203.11601 \[hep-ph\]](#).
- [57] P. Skands, S. Carrazza, and J. Rojo, *Eur. Phys. J. C* **74**, 3024 (2014), [arXiv:1404.5630 \[hep-ph\]](#).
- [58] M. Cacciari and G. P. Salam, *Phys. Lett. B* **641**, 57 (2006), [arXiv:hep-ph/0512210](#).
- [59] M. Cacciari, G. P. Salam, and G. Soyez, *Eur. Phys. J. C* **72**, 1896 (2012), [arXiv:1111.6097 \[hep-ph\]](#).
- [60] X.-N. Wang and Y. Zhu, *Phys. Rev. Lett.* **111**, 062301 (2013), [arXiv:1302.5874 \[hep-ph\]](#).
- [61] Y. He, T. Luo, X.-N. Wang, and Y. Zhu, *Phys. Rev. C* **91**, 054908 (2015), [Erratum: *Phys. Rev. C* **97**, 019902 (2018)], [arXiv:1503.03313 \[nucl-th\]](#).
- [62] S. Cao, T. Luo, G.-Y. Qin, and X.-N. Wang, *Phys. Rev. C* **94**, 014909 (2016), [arXiv:1605.06447 \[nucl-th\]](#).
- [63] S. Cao, T. Luo, G.-Y. Qin, and X.-N. Wang, *Phys. Lett. B* **777**, 255 (2018), [arXiv:1703.00822 \[nucl-th\]](#).
- [64] T. Luo, S. Cao, Y. He, and X.-N. Wang, *Phys. Lett. B* **782**, 707 (2018), [arXiv:1803.06785 \[hep-ph\]](#).
- [65] S.-L. Zhang, T. Luo, X.-N. Wang, and B.-W. Zhang, *Phys. Rev. C* **98**, 021901 (2018), [arXiv:1804.11041 \[nucl-th\]](#).
- [66] B. L. Combridge, *Nucl. Phys. B* **151**, 429 (1979).
- [67] E. Eichten, I. Hinchliffe, K. D. Lane, and C. Quigg, *Rev. Mod. Phys.* **56**, 579 (1984), [Addendum: *Rev. Mod. Phys.* **58**, 1065–1073 (1986)].
- [68] J. Auvinen, K. J. Eskola, and T. Renk, *Phys. Rev. C* **82**, 024906 (2010), [arXiv:0912.2265 \[hep-ph\]](#).
- [69] X.-f. Guo and X.-N. Wang, *Phys. Rev. Lett.* **85**, 3591 (2000), [arXiv:hep-ph/0005044](#).
- [70] X.-N. Wang and X.-f. Guo, *Nucl. Phys. A* **696**, 788 (2001), [arXiv:hep-ph/0102230](#).
- [71] B.-W. Zhang and X.-N. Wang, *Nucl. Phys. A* **720**, 429 (2003), [arXiv:hep-ph/0301195](#).
- [72] B.-W. Zhang, E. Wang, and X.-N. Wang, *Phys. Rev. Lett.* **93**, 072301 (2004), [arXiv:nucl-th/0309040](#).
- [73] B.-W. Zhang, E.-k. Wang, and X.-N. Wang, *Nucl. Phys. A* **757**, 493 (2005), [arXiv:hep-ph/0412060](#).
- [74] B. Schenke, S. Jeon, and C. Gale, *Phys. Rev. C* **82**, 014903 (2010), [arXiv:1004.1408 \[hep-ph\]](#).
- [75] B. Schenke, S. Jeon, and C. Gale, *Phys. Rev. Lett.* **106**, 042301 (2011), [arXiv:1009.3244 \[hep-ph\]](#).
- [76] J.-F. Paquet, C. Shen, G. S. Denicol, M. Luzum, B. Schenke, S. Jeon, and C. Gale, *Phys. Rev. C* **93**, 044906 (2016), [arXiv:1509.06738 \[hep-ph\]](#).
- [77] J. S. Moreland, J. E. Bernhard, and S. A. Bass, *Phys. Rev. C* **92**, 011901 (2015), [arXiv:1412.4708 \[nucl-th\]](#).
- [78] W. Ke, J. S. Moreland, J. E. Bernhard, and S. A. Bass, *Phys. Rev. C* **96**, 044912 (2017), [arXiv:1610.08490 \[nucl-th\]](#).
- [79] H. Zhang, T. Song, and C. M. Ko, *Phys. Rev. C* **87**, 054902 (2013), [arXiv:1208.2980 \[hep-ph\]](#).
- [80] J. H. Putschke *et al.*, (2019), [arXiv:1903.07706 \[nucl-th\]](#).
- [81] B. Andersson, G. Gustafson, and B. Soderberg, *Z. Phys. C* **20**, 317 (1983).
- [82] T. Sjostrand, *Nucl. Phys. B* **248**, 469 (1984).
- [83] A. Kumar *et al.* (JETSCAPE), *Phys. Rev. C* **107**, 034911 (2023), [arXiv:2204.01163 \[hep-ph\]](#).
- [84] R. Baier, Y. L. Dokshitzer, A. H. Mueller, and D. Schiff, *JHEP* **09**, 033 (2001), [arXiv:hep-ph/0106347](#).

- [85] Y. S. Lai, J. Mulligan, M. Płoskoń, and F. Ringer, *JHEP* **10**, 011 (2022), [arXiv:2111.14589 \[hep-ph\]](#).
- [86] J. Brewer, A. Sadofyev, and W. van der Schee, *Phys. Lett. B* **820**, 136492 (2021), [arXiv:1809.10695 \[hep-ph\]](#).
- [87] J. Casalderrey-Solana, Z. Hulcher, G. Milhano, D. Pablos, and K. Rajagopal, *Phys. Rev. C* **99**, 051901 (2019), [arXiv:1808.07386 \[hep-ph\]](#).
- [88] J. Brewer, Q. Brodsky, and K. Rajagopal, *PoS Hard-Probes2020*, 037 (2021), [arXiv:2009.03316 \[hep-ph\]](#).
- [89] Y.-L. Du, D. Pablos, and K. Tywoniuk, *JHEP* **21**, 206 (2020), [arXiv:2012.07797 \[hep-ph\]](#).
- [90] J. Brewer, Q. Brodsky, and K. Rajagopal, *JHEP* **02**, 175 (2022), [arXiv:2110.13159 \[hep-ph\]](#).
- [91] J. Brewer, J. G. Milhano, and J. Thaler, *Phys. Rev. Lett.* **122**, 222301 (2019), [arXiv:1812.05111 \[hep-ph\]](#).
- [92] A. Takacs and K. Tywoniuk, *JHEP* **10**, 038 (2021), [arXiv:2103.14676 \[hep-ph\]](#).
- [93] S. Wang, J.-W. Kang, W. Dai, B.-W. Zhang, and E. Wang, *Eur. Phys. J. A* **58**, 135 (2022), [arXiv:2107.12000 \[nucl-th\]](#).
- [94] S. Acharya *et al.* (ALICE), (2023), [arXiv:2308.16131 \[nucl-ex\]](#).
- [95] S. Acharya *et al.* (ALICE), (2023), [arXiv:2308.16128 \[nucl-ex\]](#).
- [96] M. I. Abdulhamid *et al.* (STAR), (2023), [arXiv:2309.00156 \[nucl-ex\]](#).
- [97] M. I. Abdulhamid *et al.* (STAR), (2023), [arXiv:2309.00145 \[nucl-ex\]](#).
- [98] J. Yan, S.-Y. Chen, W. Dai, B.-W. Zhang, and E. Wang, *Chin. Phys. C* **45**, 024102 (2021), [arXiv:2005.01093 \[hep-ph\]](#).
- [99] J.-W. Qiu, F. Ringer, N. Sato, and P. Zurita, *Phys. Rev. Lett.* **122**, 252301 (2019), [arXiv:1903.01993 \[hep-ph\]](#).
- [100] J.-W. Qiu, F. Ringer, N. Sato, and P. Zurita, *Nucl. Phys. A* **1005**, 121853 (2021), [arXiv:2002.01652 \[hep-ph\]](#).
- [101] A. Hayrapetyan *et al.* (CMS), *Phys. Lett. B* **861**, 139088 (2025), [arXiv:2405.02737 \[nucl-ex\]](#).
- [102] S. Wang, Y. Li, J.-W. Kang, and B.-W. Zhang, (2024), [arXiv:2408.10924 \[hep-ph\]](#).